Interaction process between gaseous CH 3 I and NaCl particles: implication for iodine dispersion in the atmosphere

Hanaa Houjeij, Anne-Cécile Gregoire, Gwenaëlle Le Bourdon, Laurent Cantrel, Sophie Sobanska

Interaction process between gaseous CH_3I and NaCl particles: implication for iodine dispersion in the atmosphere

Hanaa Houjeij[a,b], Anne-Cécile Gregoire[b*], Gwenaëlle Le Bourdon[a], Laurent Cantrel[b] and Sophie Sobanska[a*]

[a] *Institut des Sciences Moléculaires, Université de Bordeaux, UMR CNRS 5255, 33405 Talence Cedex, France*

[b] *Institut de Radioprotection et de Sûreté Nucléaire (IRSN), PSN-RES, SEREX, Laboratoire expérimentation environnement et chimie (L2EC) 13115 St Paul Lez Durance, France*

**corresponding authors: sophie.sobanska@u-bordeaux.fr; anne-cecile.gregoire@irsn.fr*

Abstract

Gaseous iodomethane (CH_3I) is naturally emitted into the atmosphere by biological activity in the oceans and during a severe accident (SA) of a nuclear power plant. In this later case, a part of radioactive iodine as ^{131}I, may be released. Improving the knowledge of the CH_3I transport and reactivity in the atmosphere is important since they are strongly linked to first, the cycle of ozone and second to the dispersion of radioactive CH_3I with potential radiological consequences on both environment and human health. Here, the interaction process of CH_3I with NaCl as surrogate of atmospheric aerosols was investigated at ambient air conditions by using Diffuse Reflectance Fourier Transform Spectroscopy (DRIFTS). The DRIFTS spectra of NaCl clearly evidenced CH_3I adsorption on the NaCl particle surface. A part of CH_3I ($(1.68\pm 0.85) \times 10^{14}$ molecule.mg^{-1}_{NaCl}) was found to be strongly bonded to NaCl since no desorption was observed. The CH_3I adsorption on NaCl surface presented a 1^{st} order kinetics relative to its gas phase concentration. The uptake coefficient was determined to be in the order of 10^{-11}. These results show a low probability of CH_3I to be taken up by halide-containing aerosols. These data are crucial for completing the iodine atmospheric chemical scheme.

1. Introduction

Gaseous organic iodine species (CH_3I, ^{127}I) are naturally emitted at trace level (maximum at 2000 ppt) into the atmosphere over oceans through the algae and phytoplankton activities [1,2]. Iodine has a strong interest in the atmospheric chemistry field. Over the last four decades, numerous experimental and theoretical works have been carried out on the quantification of iodine forms (gaseous or particulate) in the troposphere, on the identification of natural sources of iodine and finally on its reactivity, with the aim of better understanding the iodine cycle and its interaction with other compounds present in the troposphere [3,4]. In that atmospheric context, many gas phase mechanisms of iodine have been developed and a large database of the iodine cycle data is now available [1–6]. However, the interaction of gaseous iodine compounds with atmospheric aerosols and its resulting speciation are not well documented, yet. Indeed, only few laboratory studies have investigated the interaction of iodinated species with atmospheric aerosols surrogates. For instance, it was found that HOI can react with NaCl and NaBr to form ICl or IBr in gaseous phase in the 5-25 °C temperature range [7]. The measured steady state uptake coefficient was determined to be in the order of 10^{-2}. Similarly, uptake of CH_3I [8] and C_2H_5I [9] by commercial soot film and carbon thin film, respectively, was determined to be in the order of 10^{-2} at 25°C. Most of the studies imply that iodine species are highly reactive and may interact with the other species (gas or particles) present in the atmosphere to evolve in gaseous or particulate form. However, neither uptake processes nor influence of condensed phase on gaseous iodine reactivity, were unravelled.

Following a severe accident on a nuclear reactor as Three Mile Island (USA, 1978), Chernobyl (Ukraine, 1986), and more recently Fukushima (Japan, 2011), iodine radioactive -isotopes (as ^{131}I, half-life of 8.02 days) produced by the fuel fission, may be released into the atmosphere mainly under gaseous (mainly I_2 and RI – R = alkyl group/chain type CH_3I) or aerosol (CsI) forms [10,11]. Particularly, gaseous CH_3I is mainly a product of the reaction between I_2 and carbon-based materials such as epoxy paints existing in the nuclear reactor building. Among released iodine species, CH_3I is the most challenging to be filtrated by the current mitigation systems (such as metallic filters, aqueous scrubbers, or sand bed filters) [12–14]. Radioactive isotopes of iodine (as ^{131}I) are highly toxic to human health due to its easy and almost irreversible transport to the human thyroid gland, where it can locally induce cancer [15,16]. Indeed, after the accident of Chernobyl and Fukushima, near field activity concentrations of ^{131}I in air was found to be 750,000 Bq.m^3 (~0.03 ppt) and 5600 Bq.m^3 (~0.0002 ppt), respectively [17]. Previous study have shown that ^{131}I was dispersed to a long distances i.e., >3000 km in the atmosphere after Chernobyl and Fukushima severe nuclear accidents[17]. Moreover, it should be noted that local meteorological conditions can cause a great variability in activity concentrations in environmental media and can result in locations further away being higher in concentration than closer locations [17–20]. With this intention, the French Institute of Radioprotection and Nuclear Safety (IRSN) has

developed specific simulation software's (C^3X plateform) which is capable of reproducing the release and dispersion of the radionuclides in the atmosphere [21–23]. However, one potential problem with such simulation tool is that the transport of ^{131}Iodine products following an accident is currently modelled without considering the physical/chemical evolution of iodine in the atmosphere, i.e. the gas phase evolution or interaction with atmospheric aerosols even if recent works [24] focused on organic reactivity in the field of nuclear accident.
To the best of our knowledge, there is no literature report about the uptake coefficient of methyl halides (CH_3Br, CH_3Cl, CH_3I) by atmospheric aerosols. Hence, to date, the heterogeneous reactivity of CH_3I in the atmosphere is not fully accounted by the atmospheric community, nor in the field of nuclear safety. This is worrisome because the simulated atmospheric dispersion of radioactive isotopes of iodine [20,25,26] may be quite different from the actual one due to the different possible fates of iodine within the Earth's atmosphere.

Thus, in this study interest was brought on gaseous CH_3I interaction with atmospheric aerosols, which may affect the chemical form of iodine in the atmosphere and thus, their atmospheric fate and dispersion. Studying sea salt aerosols is particularly significant since first, CH_3I is naturally emitted by ocean surface and second, sea salt particles are well known as reactive surfaces for heterogeneous and multiphase chemical reactions for both inorganic and organic gases[27,28]
In this work, the adsorption of CH_3I on sea salt particle surrogates (NaCl, KBr and NaI) were investigated by using the diffuse reflectance infrared Fourier transform spectroscopy (DRIFTS) technique. Solid sodium chloride as the main sea salt component was firstly considered (NaCl). Then after potassium bromide (KBr) and sodium iodide (NaI) were used in the view of investigating the influence of halide atom on the interaction process. The evolution of FTIR spectra of CH_3I in interaction with solids was followed as function of time. The capability of desorption of CH_3I from salts was also explored. Considering the importance of this interaction on the dispersion of gaseous CH_3I in the atmosphere, the uptake coefficient was determined. Owing to the adsorption process of CH_3I on sea salt particle surrogates investigated here, the knowledge on the fate and dispersion of CH_3I in the atmosphere could be further completed.

2. Materials and methods

2.1 Chemicals

Methyl iodide 1000 ppm (0.1% CH_3I, 99.9% Ar) and Argon (99.99% pure) gas bottles were provided from commercial cylinders Air product and Air liquid, respectively. The gases were used without any further purification. For the experiments, commercial powdered solids were used: sodium chloride (NaCl, 99.99%, ALFA AESAR), potassium bromide (KBr, 99+%, SIGMA ALDRICH) and sodium iodide (NaI, 99+%, ACROS).
Before each experiment, the salt sample was manually grinded and then preheated for a minimum of 4 hours at 600 °C to remove water and pre-adsorbed species (impurities) on the powder surface. The granulometry of the grinded powders was estimated by mechanical sieving on a series of 4 grids allowing to sort out the granulometry from 300 µm down to less than 50 µm. For NaCl, the particles with size ranges 300-100 µm, 100-60 µm, 60 -50 µm, and <50 µm accounted for 32%, 26%, 39% and 3% in mass, respectively. A similar granulometry distribution was found for NaI and KBr grinded salt powders.
The Specific surface area of grinded NaCl was determined on a Nitrogen sorption Micromeritics ASAP 2010 analyzer by using the Brunauer-Emmett-Teller (BET) method. The BET surface area was found to be low (0.26 $m^2.g^{-1}$), in the same order of magnitude as BET surface area previously determined for NaCl powder (0.68 $m^2.g^{-1}$) [29]. The BET surface area of NaI and KBr was assumed to be close to that of NaCl. The low BET surface area indicated that these solids were non-porous and that the available surface area was very low for colliding with trace gas phase species.

2.2 *In Situ* Diffuse Reflectance Fourier Transform Spectroscopy (DRIFTS) experiments

The continuous, *in situ*, monitoring of-solids was performed in a DRIFTS cell (Harrick, Praying Mantis™ High Temperature Reaction Chambers, 24V, HVC-DRP-4) with an interior volume of 15.78 ml equipped with Zinc selenide (ZnSe) windows. The DRIFTS cell was housed in an FTIR-spectrometer (Nicolet 6700 - Thermo Optek) equipped with a high sensitivity deuterated triglycine sulfate (DTGS) detector. The cell can be temperature controlled in the 23-400 °C range. The Cell temperature was monitored by a K-type thermocouple. The relative humidity (RH) and temperature were continuously measured using a RH/T° sensor (SHT75 Sensirion) placed on the line before the DRIFTS cell.
For each experiment, a known mass of powdered salts (close to 145 mg for each experiment) was placed in the crucible (6.3 mm internal diameter and 3.18 mm high) of the DRIFTS cell without using a packing device. The DRIFTS

cell was purged with argon at 23°C for 10 minutes to remove as much as possible H_2O and gaseous impurities. Solid powder was taken as the background spectrum under Ar flow of 108 mL.min^{-1}.
Four series of experiments were conducted as described below:
(1) NaCl was exposed continuously to an Argon/CH_3I flow (108 mL.min^{-1}) with a CH_3I concentration of 1000 ppm during 5 hours (named *Exposure phase*). Then after, the Ar/CH_3I flow was stopped, the DRIFTS cell was closed and desorption of sorbed species was monitored for 1 hour (named *Spontaneous desorption phase*). An additional step in dynamic condition consisted in flowing pure Ar (108 mL.min^{-1}) up to 1 hour (named *Induced desorption phase*). Experiments were performed under ambient conditions (% RH=20%) at 23 °C and 1 atm. Each experiment was repeated three times.
Although not atmospherically relevant, the excess of CH_3I regarding the solid i.e. the concentration of 1000 ppm was chosen in a first approach for our experiments in order to ensure the detection of reaction species if any. The influence of CH_3I concentration on uptake coefficient is explored in the following.
(2) Desorption process was thermally activated by increasing the temperature up to 350 °C under Ar flow (named activated desorption phase). In this view, NaCl was firstly exposed to Ar/CH_3I flow (108 mL.min^{-1}, CH_3I 1000 ppm) for 1 hour under % RH=20% at 23°C and 1 atm (*Exposure phase*). In a second step, the DRIFTS cell was closed and spontaneous desorption was monitored for 4 hours. In a last step, desorption was monitored in dynamic conditions under Ar flow (108 mL.min^{-1}) for 1 hour still at 23 °C (*Induced desorption phase*). Finally, the temperature was gradually increased up to 100, 200 and finally 350 °C under the same Ar flow (named activated desorption phase). A heating rate of 3 K.min^{-1} was applied with a dwell of 15 minutes at each target temperature.

(3) The third series of experiments aimed to investigate the influence of CH_3I gas phase concentration on the CH_3I sorption process on NaCl under % RH=20% at 23°C and 1 atm. Similar to the first series of experiments, NaCl was exposed to a continuous flow of CH_3I of 500 and 200 ppm maintained at 108 mL.min^{-1} for 5 hours. No spontaneous, induced or activated desorption phases were applied in this scenario.

(4) Finally, the four series of experiments considered the nature of the halide salts (NaI and KBr) on CH_3I sorption compared to NaCl. Experiments were limited to the exposure phase (CH_3I at 1000 ppm in argon for a total flow of 108 ml/min at 23°C) and for a test duration of 1 hour.
Experimental conditions of the series of experiments performed in this study were summarized in Table S1 in supporting information.

For the whole experiments, the infrared spectra were recorded as a function of time in the spectral range from 4000 to 600 cm^{-1} with a resolution of 8 cm^{-1}. Each spectrum was an average of 200 scans featuring a spectral sampling frequency of 7-8 spectra/hour. Note that the C-I stretching mode at 572 cm^{-1} cannot be observed because ZnSe window cuts the spectrum between 16000-600 cm^{-1}. The background subtraction was achieved by the Omnic software for each spectrum. The baseline was corrected by linear interpolation model using Omnic software. The DRIFTS spectra were reported as log ($1/R_\infty$) (pseudo-absorbance), where R is the diffuse reflected signal. Note that this pseudo-absorbance gives a better linear representation of DRIFTS band intensity against the adsorbate surface concentrations than that given by Kubelka–Munk function for poorly absorbing adsorbates [30]. A band decomposition of the overlapped bands was accomplished by Gaussian function multiple band with Levenberg-Marquardt mathematical model using FityK software [31]. Absolute uncertainty of the band area in the 1400-1000 cm^{-1} was found between ~ 0.03 to 0.37 arbitrary units at 95% confidence level.

2.3 Analysis of solids

After each DRIFT experiments, the total amount of iodine (I) adsorbed on NaCl was determined by Inductively Coupled Plasma Mass Spectrometer (ICP-MS, 810 MS VARIAN). The detection limit of 3 µg.L^{-1} was determined for iodine element [32]. Two thirds of the NaCl powder samples were dissolved instantly after exposure to 5 hours of continuous CH_3I flow (1000 ppm, 108mL.min^{-1}), by NaOH (0.1 mol.L^{-1}) for analysis. The total amount of iodine (I) adsorbed on NaCl could be thus determined.

3. Results and discussion

To investigate the influence of the interaction of CH_3I with sea salt surrogates on the dispersion of CH_3I in the atmosphere, the following sections examine: (1) the sorption process of CH_3I on NaCl, (2) the evolution of adsorbed CH_3I on NaCl over time, (3) the kinetics of adsorption process of CH_3I on NaCl and the influence of temperature, concentration and nature of halide salts on this process and finally (4) the uptake coefficient determination.

3.1 Spectroscopic evaluation of the adsorption of CH_3I on NaCl at 23 °C and %RH=20%

A representative spectrum of NaCl exposed to CH_3I during 5 hours and recorded in the mid IR region (4000-600 cm^{-1}) is shown in Figure 1. Three typical regions assigned to CH_3 stretching, CH_3 deformation and CH_3 rocking were observed (Figure 1). The detailed description of the CH_3 stretching (3050-2800 cm^{-1}) and CH_3 deformation (1500-900 cm^{-1}) for a proper assignment is given below. In the CH_3 rocking (900-700 cm^{-1}) spectral region the bands observed were not resolved enough to be properly assigned.

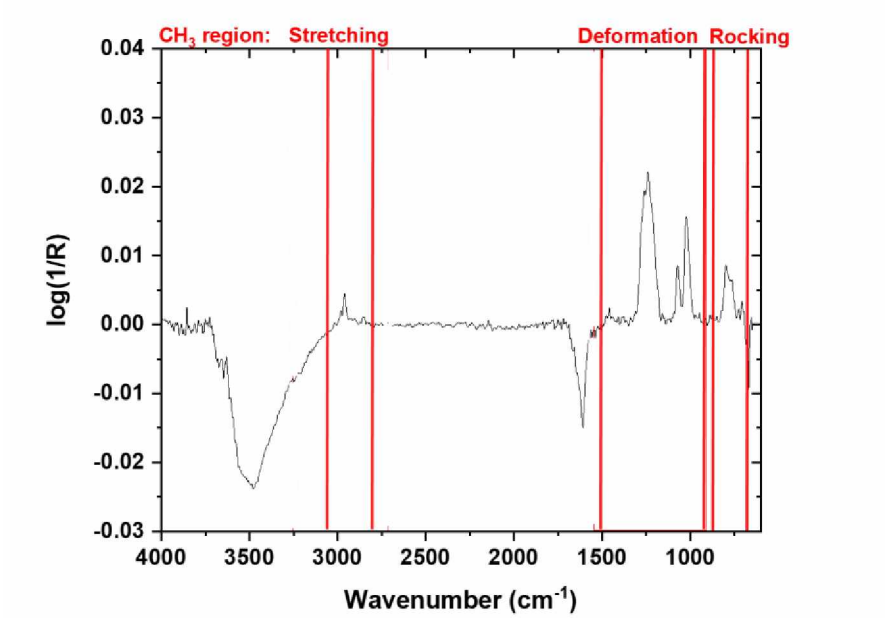

Figure 1 Typical DRIFTS spectra in mid IR spectral range [4000-600 cm^{-1}] of NaCl exposed to 5 hours of CH_3I flow (108mL.min^{-1}, 1000 ppm) at 23°C and 1 atm. (The two negative broad bands around 3500 cm^{-1} and 1600 cm^{-1} are related to H_2O peaks derived from the baseline correction).

In the CH_3 stretching region (3050-2800 cm^{-1}) shown in Figure 2(a), bands at 3018, 2993, 2981, 2961, 2855 and 2847 cm^{-1} were observed. Overlapped bands in the 2961 cm^{-1} region were decomposed using Gaussian function into two bands at 2961 and 2953 cm^{-1} (Figure 2(c)). The IR bands observed at 2981, 2953, and 2847 cm^{-1} were assigned to the characteristic bands of CH_3I in gas phase (see bands marked in green in the Figure 2(a)) as described in the literature [33,34]. The bands at 2981, 2953 and 2847 cm^{-1} were attributed to the CH_3 asymmetric stretching, CH_3 symmetric stretching and overtone modes of CH_3I in gas phase, respectively. Gaseous CH_3I remaining near the NaCl surface were detected by DRIFTS measurement. Based on the IR bands observed for CH_3I adsorbed on titanium oxide [33] and silver zeolites [34], the bands observed at 3018, 2961 and 2855 cm^{-1} (marked in blue in Figure 2(a)) were assigned as characteristic bands for CH_3I adsorbed on NaCl. The frequencies were attributed to CH_3 asymmetric stretching, symmetric and overtones modes of adsorbed CH_3I, respectively. This is consistent with a blue shift of the CH_3 asymmetric stretching (37 cm^{-1}), symmetric stretching (8 cm^{-1}) and asymmetric overtone (8 cm^{-1}) modes of CH_3I related to gaseous species. Additionally, a low intensity band at 2993 cm^{-1} was observed and can be also attributed to the interaction of CH_3I with NaCl. Actually, compared to CH_3I adsorbed on Si [35] and Cu [36] surfaces, the stretching mode of CH_3 varied between 3080 and 2909 cm^{-1}. Thus, 2993 cm^{-1} can be tentatively attributed to the CH_3 stretching of adsorbed CH_3I. The observation of two bands i.e. at 2993 and 2961 cm^{-1} for the same CH_3 stretching mode might be explained with different geometrical adsorbed structures of CH_3I on NaCl surface.

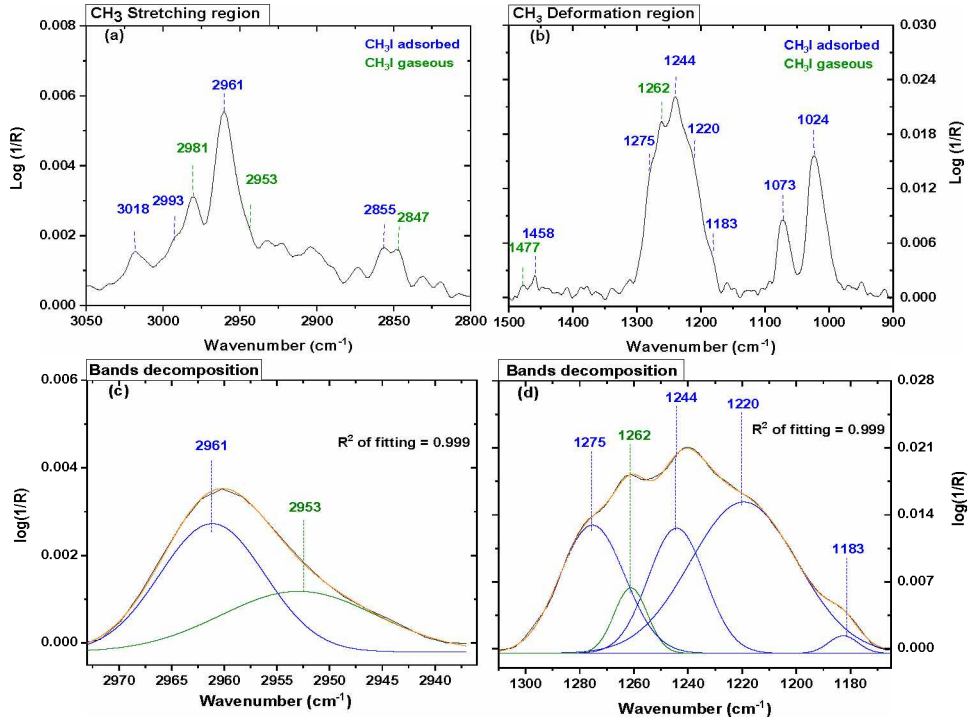

Figure 2 DRIFTS spectra of NaCl exposed to 5 hours of CH_3I (108mL.min^{-1}, 1000 ppm) continuous flow at 23°C and 1 atm (a) in the 3050-2800 cm^{-1} (b) in the 1500-900 cm^{-1} (c) in the 2963-2935 cm^{-1} (d) in the 1305-1160 cm^{-1} IR spectral range. Bands was decomposed with Gaussian function using FityK software. Blue bands are CH_3I adsorbed on NaCl and green bands are CH_3I in gas phase near the NaCl surface.

In the CH_3 deformation region (1500-900 cm^{-1}), bands at 1477, 1458, 1262, 1244, 1073 and 1024 cm^{-1} were observed (Figure 2(b)). Based on the literature [33,34] the bands at 1477 and 1262 cm^{-1} were assigned to the CH_3 asymmetric and symmetric deformations of gaseous CH_3I which was consistent with the frequencies reported for the CH_3 stretching region of gaseous CH_3I. Based on previous study [33], the band at 1458 cm^{-1} (Figure 2(b)) was attributed to the CH_3 asymmetric deformation of adsorbed CH_3I. In this spectral region, the band centered at 1244 cm^{-1} evidenced some shoulders; the decomposition of this band and the fitting procedure using Gaussian function allowed to extract the additional bands at 1275, 1220 and 1183 cm^{-1} (see Figure 2(d)). Similar shoulder were clearly observed in previous works although they were not assigned [33,34]. As previously reported [31–37][33-39], the CH_3 symmetric deformation of the CH_3I can shift (red and blue shift) from 1190 cm^{-1} to 1250 cm^{-1} depending on the type of solid or on the orientation of the crystallographic planes of single metallic solids. This strongly suggest that the bond geometries of the adsorbed CH_3I on NaCl are a key for understanding adsorption of CH_3I on salts and their subsequent reactivity which can highly affect the observed vibrational modes.

In addition, two intense bands at 1073 and 1024 cm^{-1} were observed (Figure 2(b)). These bands were not reported in the literature for CH_3I molecules adsorbed on surfaces. Based on their band wavenumbers they can be assigned to CH_2I_2 [40-42], CH_3OH [34] or CH_3Cl [43-45]. The hypothesis of formation of such species on NaCl was discarded because experimental conditions required to form such species were drastically different in term of temperature or surfaces, compared to the conditions used in our experiments. The SN_2 halide substitution at NaCl surface suggested by Gu et al., [45] in a theoretical study was not consistent with our results obtained with NaI surface. Indeed, the exposure of NaI to CH_3I conducted with similar experimental conditions, yielded to the same FTIR spectrum with new bands at 1073 and 1024 cm^{-1} (Figure S1). In consequence, a non-described adsorption geometry of CH_3I at the surface was hypothesized.

These intense bands in the CH_3 deformation region at 1073 and 1024 cm^{-1} (Figure 2(b)) were strongly red shifted compared to the CH_3 deformation band of free CH_3 at 1262 cm^{-1} with values at -189 and -238 cm^{-1}, respectively. These latter suggest a strong interaction of CH_3I with NaCl surface. It was reported [37-39], that with low coverage, CH_3I adsorbed on single metallic surface was of C_3 symmetry. However, with higher coverages a geometrical rearrangement occurs until C-I bond becomes aligned with the surface maintaining C_3v symmetry in binding to the surface. In contrary to powdered sample, a single crystal sample has a continuous, unbroken and free of defects lattice. Additional Density Functional Theory calculations (See Supporting Information) of CH_3I monomer has shown that iodomethane dipole moment was oriented toward carbon atom, which leads to a partial negative Mulliken's charge for carbon atom and partial positive Mulliken's charge for hydrogen and iodine atoms as shown in Figure 3. Assuming that CH_3I was adsorbed on NaCl with a C_3v configuration as shown in Figure 3, then we may expect an attraction of hydrogen atoms toward chloride atoms at the surface of NaCl due to charge difference. The observation of two bands for this

configuration probably reflects the non-equivalent hydrogen atoms attached to the Cl on NaCl surface. Moreover, the electronegativity of chloride atom is higher than iodine atom, which might reveal a strongest interaction of hydrogen atom with iodine ion (weakest ionic bonding). Thus, one would expect more than one geometrical orientation of adsorbed CH_3I with powdered NaCl sample. This highly reflects the observation of more than one band for CH_3 symmetric deformation and symmetric stretching modes of adsorbed CH_3I on halide salts. Thus, the new intense bands were assigned to the unique C_3v geometrical adsorption of CH_3I that occurs specifically with halide salt surfaces. This geometry was not described in the literature.

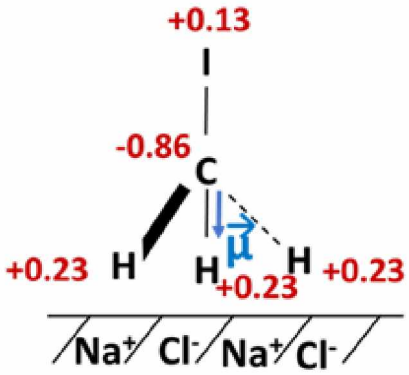

Figure 3 Scheme of CH_3I monomer adsorption on NaCl and Mulliken charge distribution calculated with DFT performed using ωB97XD/aug-cc-pVTZ-PP level of theory.

Experimental wavenumbers observed from the interaction of CH_3I on halide salts (NaCl, NaI and KBr) and respective assignments were summarized in Table 1.

Table 1 Tentative assignment of the observed IR absorption bands in cm^{-1} of CH_3I in gas (g) and adsorbed (ads) on the surface of halide salts (NaCl, NaI and KBr) under %RH=20% at 23°C and 1 atm.

Experimental wavenumber (cm^{-1})	Assignement	corresponding species
3018	CH_3 asymmetric stretching	$CH_3I_{(ads)}$
2993	CH_3 symmetric stretching	$CH_3I_{(ads)}$
2981	CH_3 asymmetric stretching	$CH_3I_{(g)}$
2961	CH_3 symmetric stretching	$CH_3I_{(ads)}$
2953	CH_3 symmetric stretching	$CH_3I_{(g)}$
2855	CH_3 overtone	$CH_3I_{(ads)}$
2847	CH_3 overtone	$CH_3I_{(g)}$
1477	CH_3 symmetric deformation	$CH_3I_{(g)}$
1458	CH_3 asymmetric deformation	$CH_3I_{(ads)}$
1275	CH_3 asymmetric deformation	$CH_3I_{(ads)}$
1262	CH_3 symmetric deformation	$CH_3I_{(g)}$
1244	CH_3 symmetric deformation	$CH_3I_{(ads)}$
1220	CH_3 symmetric deformation	$CH_3I_{(ads)}$
1183	CH_3 symmetric deformation	$CH_3I_{(ads)}$
1073	CH_3 symmetric deformation	$CH_3I_{(ads)}$
1024	CH_3 symmetric deformation	$CH_3I_{(ads)}$

3.2. Time evolution of CH_3I adsorption and desorption on NaCl

The time evolution of CH_3I amount adsorbed or desorbed on NaCl surface was evaluated by following the sum of the band areas related to $CH_3I_{(ads)}$ (i.e. bands at 1275, 1244, 1220, 1183, 1073 and 1024 cm^{-1} labelled as $\sum CH_3I_{adsorbed}$ in the following*)*. Time evolution in the CH_3I deformation region (1400-900 cm^{-1}) is reported in Figure S2 for the CH_3I exposure phase and in Figure S3 for the spontaneous and induced desorption phases for experiment series (1)

The evolution of band area of the band at 1262 cm^{-1} related to gaseous phase, is stable over time in both CH_3I exposure and spontaneous desorption phases (Figure 4). The complete disappearance of the IR bands related to gaseous CH_3I during Ar flow (Figure 4(a)) indicates the presence of gaseous CH_3I near NaCl surface. The evolution of the bands related to adsorbed CH_3I ($\Sigma CH_3I_{adsorbed}$) is reported in Figure 4 (b). The $\Sigma CH_3I_{adsorbed}$ bands increases during the CH_3I exposure phase to reach an apparent plateau with no apparent desorption in both spontaneous and induced desorption phases.

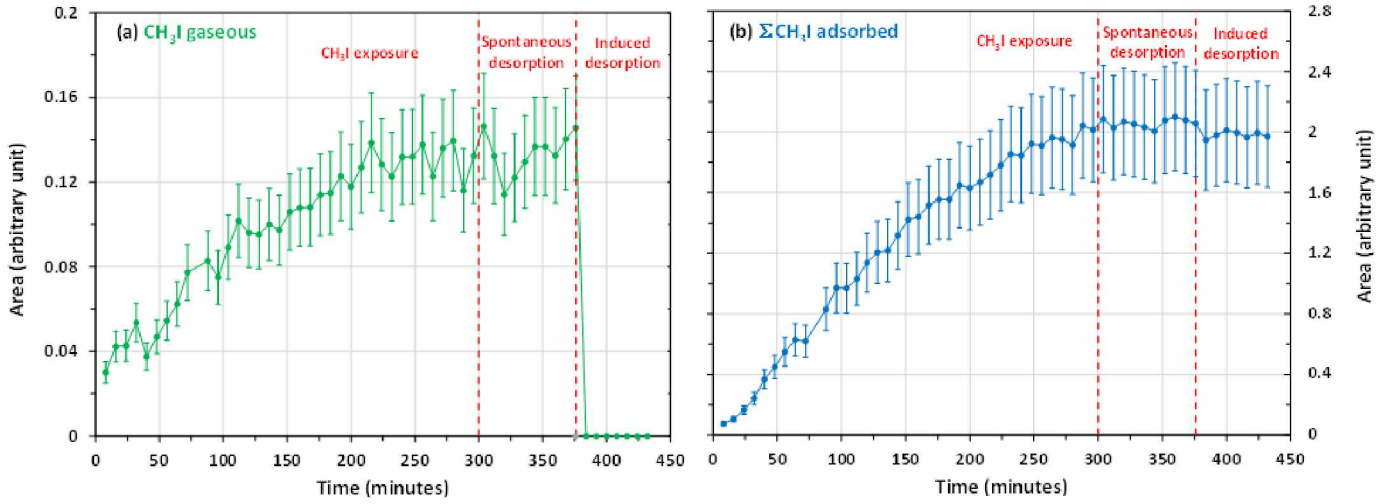

Figure 4 Area of the (a) CH_3I gaseous band and (b) $\Sigma CH_3I_{adsorbed}$ bands as a function of time during CH_3I exposure, spontaneous and induced desorption phases. Exposure phase denotes the continuous flow of 108 mL.min^{-1} of CH_3I (1000 ppm) on NaCl. The spontaneous desorption phase denotes the static conditions after 5 hours of CH_3I flow and induced desorption phase denotes the continuous pure Ar flow after the static condition.

In order to activate the desorption process (if any) of adsorbed CH_3I, NaCl sample was heated until 350 °C, at a rate of 3K.min^{-1} , under argon flow (experiment series (2)). The heating step occurred at 23 °C after CH_3I exposure, spontaneous and induced desorption phases which lasted for 1, 4 and 1 hour, respectively. Spectra were recorded at 100, 200 and 350 °C. The evolution of deformation band intensity during the heating steps did not show significant changes (see Figure S4 in SI). This result would indicate the non-desorbing capability of CH_3I under different static, Ar flow and temperature conditions when adsorbed on NaCl surface.

3.3 Kinetic adsorption of CH_3I on halide salts and influence of CH_3I concentration

During the CH_3I exposure phase, the evolution of the adsorption versus time is interpolated by a linear function and the rate (k) of methyl iodide adsorption can then be determined from the linear interpolation of the adsorption band area curve versus time. The average rate of adsorption (k) was determined for various concentration of CH_3I (experiment series 3) and presented in Figure 5. The average rate of adsorptions were repeatable with values of k = (6.91±0.23) ×10^{-3} arbitrary unit.min^{-1}, (3.91±0.05) ×10^{-3} arbitrary unit.min^{-1} and (1.54±0.06) ×10^{-3} arbitrary unit.min^{-1} for initial concentration of 1000 ppm, 500 ppm, 200 ppm, respectively. These values clearly show that adsorption rate depends on the initial concentration with a decreasing by a factor 2 and 5 when the concentration decreases from 1000 ppm to 500 and 200 ppm, respectively. Assuming that this relation can be extrapolated to the low CH_3I concentrations found in the atmosphere (i.e. atmospheric $[CH_3I]_g$ maximum is 2000 ppt [46]), a very low CH_3I adsorption may be expected with an adsorption rate expected to be diminished by a factor 5 × 10^5.

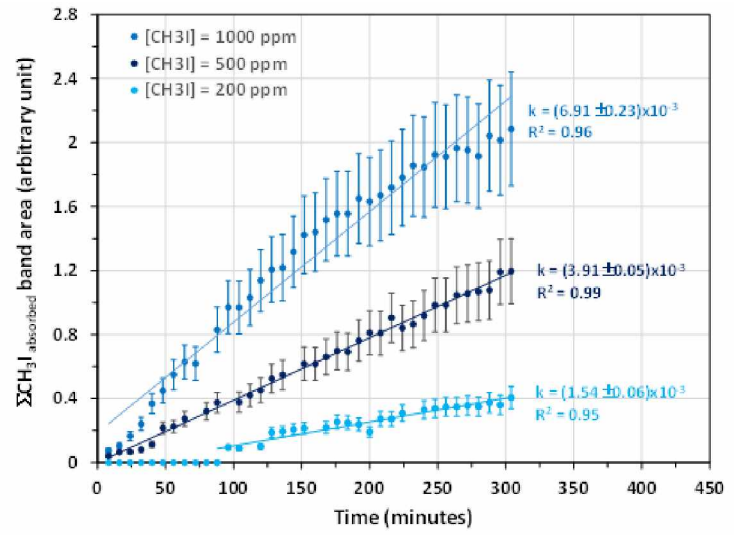

Figure 5 Area of the $\Sigma CH_3I_{adsorbed}$ bands as a function of time during exposure phase of CH_3I on NaCl. Exposure phase denotes the continuous flow of 108 mL.min^{-1} of 1000, 500 ppm and 200 ppm of CH_3I in gas phase. k= rate constant (experiment series (4)).

The rate order of adsorbed CH_3I on NaCl determined from the slope of the bi-logarithmic plot of k rate versus the concentration of CH_3I in gas phase [47,48] (see Figure S5 in SI) was estimated to be 0.84 ±0.05 indicating a first order rate for CH_3I adsorption on NaCl.

Experiments with NaI and KBr salts were conducted by continuous flow of CH_3I (108mL.min^{-1}, 1000 ppm) for 1 hour and compared to the adsorption on NaCl salt (experiment series (4)). Adsorption rate were determined for one hour test duration (Figure 6). The k rate adsorption of CH_3I on NaI and KBr are (3.10±0.87) ×10^{-2} arbitrary unit.min^{-1} and (1.53±0.31) ×10^{-2} arbitrary unit.min^{-1}, respectively. Although k estimated for NaCl and KBr are similar, the adsorption is enhanced for NaI. Seemingly, the adsorption rate increased in the following order: NaCl ≈ KBr < NaI. The change of adsorption rate with halide solid type indicates the influence of electronegativity on the adsorption of CH_3I on halide particles. Indeed, regarding the Mulliken's charge distribution calculated for CH_3I monomer (see § 3.1), a strongest interaction is expected with iodine compared to chlorine and bromine.

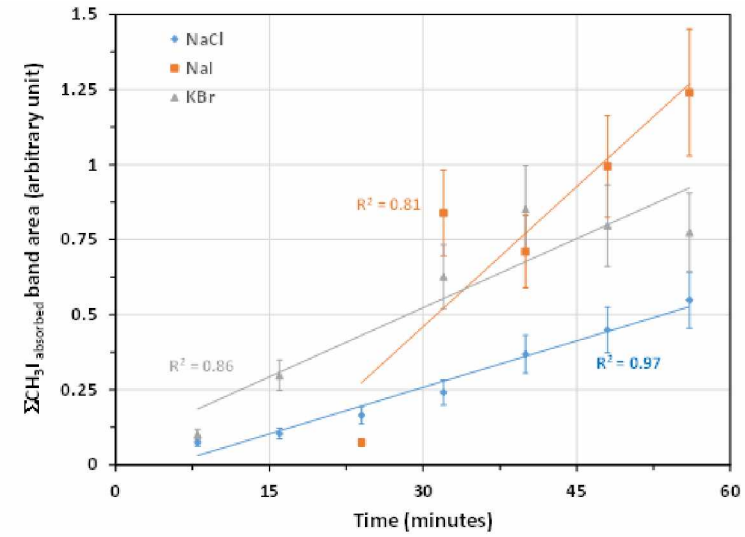

Figure 6 Area of the $\Sigma CH_3I_{adsorbed}$ bands as a function of time during exposure phase of CH_3I on NaCl, NaI and KBr. Exposure phase denotes the continuous flow of 108 mL.min^{-1} of CH_3I (1000 ppm).

3.2 Determination of uptake coefficients

The CH_3I concentration on the solid was determined by ICP-MS assuming that the overall amount of adsorbed iodine is in CH_3I form. The average concentration of iodine found in NaCl exposed to CH_3I (1000 ppm) during 5h (test series (1)) amounts up to (1.68± 0.86) × 10^{14} molecule.mg$^{-1}{}_{NaCl}$ (Table S3). Taking into account the total mass of NaCl involved in the experiment, the total amount of adsorbed CH_3I (noted $\{CH_3I_{ads}\}$) can thus be determined. Comparing the total amount of injected gaseous CH_3I_g during

the exposure phase to the total amount of adsorbed CH_3I_{ads} on NaCl, it is found that only $3x10^{-3}$ % of initially injected methyl iodide was adsorbed on NaCl as shown in Table 2, indicating a very low residual amount of CH_3I on NaCl.

Table 2 Calculation of %{CH_3I} residual on NaCl for experiment series (1) 5h exposition of NaCl to 1000 ppm CH_3I corresponds to $8.03 x10^{20}$ injected gaseous CH_3I molecules.

Test repeat	Total amount of adsorbed CH_3I {CH_3I_{ads}} in molecules	% of CH_3I residual on NaCl ={CH_3I_{ads}} / $(CH_3I)_g \times 100$
Repeat 1	$(2.05 \pm 0.16) \times 10^{16}$	2.55×10^{-3} %
Repeat 2	$(2.36 \pm 0.19) \times 10^{16}$	2.94×10^{-3} %
Repeat 3	$(3.00 \pm 0.24) \times 10^{16}$	3.74×10^{-3} %

For a quantitative interpretation of the observed IR bands in terms of amount of methyl iodide taken up by NaCl, the area of the bands assigned to adsorbed methyl iodide was assumed to be proportional to the total amount of iodine taken up by NaCl (pseudo absorbance equation [30]). Typical FTIR bands of adsorbed iodine were assumed to represent the overall amount of adsorbed CH_3I determined by ICP-MS analysis (see experimental section). The band area of the $\Sigma CH_3I_{adsorbed}$ bands was therefore translated from arbitrary unit absorbance of the spectrum to the total amount of iodine taken up by NaCl by a conversion factor (eq. 1). Based on the experiment series (1), an average conversion factor (F) of $(1.14 \pm 0.37) \times 10^{16}$ at 95% confidence level could be determined (Table S3).

$$F = \frac{\text{Total amount of iodine taken by total solid}}{\text{Band area}} \quad [1]$$

The uptake coefficient, ɣ, is defined as the ratio of the gas-surface collision rate to the total gas-surface collision rate [31,48,49]. Saturation effect phase have been hardly reached after 5 hours of continuous CH_3I exposure time (see Figure 4). Thus, the uptake in this work can be assumed as an average uptake during the 5 hours of CH_3I exposure and was determining as follow:

$$\gamma = \frac{d\{CH_3I\}}{dt} \times \frac{1}{Z} \quad [2]$$

$$Z = \frac{1}{4} \omega A [CH_3I]_g \quad [3]$$

$$\omega = [8RT/(\pi M)]^{1/2} \quad [4]$$

Where $d\{CH_3I\}/dt$ was the surface adsorption rate of CH_3I on NaCl, $[CH_3I]_g$ denoted the concentration of CH_3I (molecule.m^{-3}) in the gas phase under 5 hours of constant flow, ω was the mean thermal velocity of CH_3I (210 m.s^{-1}) and A was the effective surface area (BET surface area × mass of NaCl).

The uptake values in the range of 10^{-11} were obtained under CH_3I gaseous concentrations of 1000, 500 and 200 ppm (Table 3). These values were much lower than those reported previously about the uptake coefficient of HOI, $HOI/IONO_2$, ICl on halide salts [50] and of CH_3I on soot film [8] which was found to be in the order of 10^{-2} . This reflects the low colliding probability of CH_3I with NaCl compared to the high affinity of CH_3I for soot particles and to the reactivity of gaseous inorganic iodinated species (HOI, $HOI/IONO_2$, ICl) with halide particles. Assuming that uptake coefficient is independent of gaseous methyl iodide concentration, we can expect a very low methyl iodide uptake (~10^{-11}) on NaCl in atmospheric conditions i.e $[CH_3I]_g$ = 2000 ppt or nuclear severe accident conditions.

Table 3 Average uptake coefficient of CH_3I on NaCl for an exposure phase duration of 5 hours and under %RH=20% at 23°C and 1 atm.

[CH_3I] in ppm	[CH_3I] in molecule.m^{-3}	Rate of collision in molecule. s^{-1}	Adsorption rate in molecule. s^{-1}	γ_{ss}
1000	2.48×10^{22}	4.74×10^{22}	1.31×10^{12}	$(2.76 \pm 0.93) \times 10^{-11}$
500	1.24×10^{22}	2.37×10^{22}	7.40×10^{11}	$(3.17 \pm 1.05) \times 10^{-11}$
200	4.96×10^{21}	9.49×10^{21}	2.92×10^{11}	$(3.07 \pm 1.04) \times 10^{-11}$

The uptake coefficients calculated for KBr and NaI are reported in Table 4. Obviously, the initial adsorption rate of CH_3I was enhanced with NaI and its uptake coefficient is increasing by ~30 in comparison to NaCl and KBr. Once again, this trends (i.e. NaCl ≈ KBr < NaI) reflects the influence of electronegativity on the CH_3I-halide salt interaction process.

Table 4 Initial uptake coefficient of CH_3I (1000 ppm) on NaCl, NaI and KBr for an exposure phase duration of 1 hour and under %RH=20% at 23°C and 1 atm. 1000 ppm= 2.48×10^{22} molecule. m^{-3}.

Salt	[CH_3I] in molecule.m^{-3}	Adsorption rate in molecule.s^{-1}	γ_{ss}
NaCl	2.48×10^{22}	1.31×10^{12}	$(2.76 \pm 0.93) \times 10^{-11}$
NaI	2.48×10^{22}	5.89×10^{12}	$(1.24 \pm 0.81) \times 10^{-10}$
KBr	2.48×10^{22}	2.91×10^{12}	$(6.13 \pm 3.18) \times 10^{-11}$

4. Conclusion and environmental implications

The interaction of gaseous CH_3I with NaCl as surrogates of atmospheric sea salt aerosols has been investigated at 23°C and 1 atm. CH_3I adsorption was clearly observed at low humidity level NaCl (%RH=20% at 23°C). In addition to the adsorbed CH_3I bands already referenced in the literature, the DRIFTS spectra revealed the presence of new strong vibrational bands at 1073 and 1024 cm^{-1}. Owing to the inhomogeneity of the NaCl surface and to the time evolution of these bands, we assumed that these new bands were attributable to additional geometrical form of CH_3I as C_3v on NaCl surface described here for the first time. Further, CH_3I molecules seems to be strongly bonded on NaCl solid since no desorption was observed even after heating the system. We have found that the interaction is strongly related to the electronegativity of the halide. The adsorption does not depend on the initial concentration of CH_3I and the uptake coefficient reflecting the colliding probability with the surface is very low compared to inorganic iodine species. Indeed, the $\%\{CH_3I\}_{residual}$ sticks on solid NaCl was found to be 0.003%.

Though atmospheric and severe nuclear accident CH_3I concentrations, are 10^{-5}-10^{-9} lower than the concentrations used in this study experiments, a very low uptake on NaCl can be expected - at least of the same order (10^{-11}). Thus, the influence of NaCl aerosols on the behaviour of gaseous CH_3I can be considered as negligible. However, though in low amount, the irreversible character of adsorption makes it of particular importance for the dispersion of CH_3I in the atmosphere. Considering the total concentration of atmospheric iodine measured in case of SA, e.g. $75x10^{-2}$ ppt and $50x10^{-4}$ ppt for Chernobyl and Fukushima[11,17,25], respectively, a corresponding estimated amount of about $2.2x10^{-5}$ ppt and $1.5x10^{-7}$ ppt of CH_3I would be expected to be transported by sea salt aerosols. Although these concentrations seem low, this point should be deeper examinated to evaluate any influence on the atmosphere and environment contamination.

Author contribution

The manuscript was written through the contributions of all authors. All authors have given approval to the final version of the manuscript. HH, GLB performed the experiments. LC, ACG and SS designed the experiments, drafted, revised, and edited the manuscripts.

Conflict of interest

Authors declare no conflicts of interest.

Acknowledgements

Authors acknowledges funding from Region Nouvelle Aquitaine and IRSN to the SPECAERO project (grant n° 2017-1R10108-00013011). Authors wish to express thanks to Sonia Taamali and Dr Florent Louis for the discussion to perform theoretical calculations. Theoretical calculations was kindly provided by the Centre de Ressources Informatiques (CRI) of the University of Lille and the Centre Régional Informatique et d'Applications Numériques de Normandie (CRIANN).

References

1 L. J. Carpenter, S. M. Macdonald, M. D. Shaw, R. Kumar, R. W. Saunders, R. Parthipan, J. Wilson and J. M. C. Plane, Atmospheric iodine levels influenced by sea surface emissions of inorganic iodine, *Nat. Geosci.*, 2013, **6**, 108 111. DOI: 10.1038/ngeo1687.

2 A. Saiz-lopez, J. M. C. Plane, A. R. Baker, L. J. Carpenter, R. Von Glasow, C. G. Juan, G. Mcfiggans and R. W. Saunders, Atmospheric Chemistry of Iodine, *Chem. Rev.*, 2012, **112**, 1773–1804. DOI: 10.1021/cr200029u.

3 A. Saiz-Lopez, R. P. Fernandez, C. Ordóñez, D. E. Kinnison, J. C. G. Martín, J. F. Lamarque and S. Tilmes, Iodine chemistry in the troposphere and its effect on ozone, *Atmos. Chem. Phys.*, 2014, **14**, 13119–13143. DOI: 10.5194/acp-14-13119-2014.

4 W. R. Simpson, R. Von Glasow, K. Riedel, P. Anderson, P. Ariya, J. Bottenheim, J. Burrows, L. Carpenter, U. Frieß, M. E. Goodsite, D. Heard, M. Hutterli, H.-W. Jacobi, L. Kaleschke, B. Neff, J. Plane, U. Platt, A. Richter, H. Roscoe, R. Sander, P. Shepson, J. Sodeau, A. Steffen, T. Wagner and E. Wolf, Halogens and their role in polar boundary-layer ozone depletion, *Atmos. Chem. Phys.*, 2007, **7**, 4285–4403. DOI: 10.5194/acp-7-4375-2007.

5 A. Saiz-Lopez, J. M. C. Plane, C. A. Cuevas, A. S. Mahajan, J. F. Lamarque and D. E. Kinnison, Nighttime atmospheric chemistry of iodine, *Atmos. Chem. Phys.*, 2016, **16**, 15593–15604. DOI: 10.5194/acp-16-15593-2016.

6 L. J. Carpenter, Iodine in the Marine Boundary Layer, *Chem. Rev.*, 2003, **103**, 4953–4962.

7 J. C. Mossinger and R. A. Cox, Heterogeneous Reaction of HOI with Sodium Halide Salts, *Phys. Chem. Chem. Phys.*, 2001, **105**, 5165–5177.DOI: 10.1021/jp0044678.

8 W. Wang, M. Ge, Y. Tian and L. Yao, A flow tube study of methyl iodine uptake on soot surface, *Chem. Phys. Lett.*, 2007, **440**, 348–351.DOI: 10.1016/j.cplett.2007.04.053.

9 Y. Shi, W. Weigang and G. MaoFa, The uptake of ethyl iodide on black carbon surface, *Chinese Sci. Bull.*, 2008, **53**, 733–738.DOI: 10.1007/s11434-007-0488-2.

10 S. Dickinson, A. Auvinen, Y. Ammar, L. Bosland, B. Clément, F. Funke, G. Glowa, T. Kärkelä, D. A. Powers, S. Tietze, G. Weber and S. Zhang, Experimental and modelling studies of iodine oxide formation and aerosol behaviour relevant to nuclear reactor accidents, *Ann. Nucl. Energy*, 2014, **74**, 200–207.DOI: 10.1016/j.anucene.2014.05.012.

11 L. S. Lebel, R. S. Dickson and G. A. Glowa, Radioiodine in the atmosphere after the Fukushima Dai-ichi nuclear accident, *J. Environ. Radioact.*, 2016, **151**, 82–93.
DOI: 10.1016/j.jenvrad.2015.06.001.

12 L. Bosland, L. Cantrel, N. Girault, B. Clement, L. Bosland, L. Cantrel, N. Girault and B. Clement, Modeling of Iodine Radiochemistry in the ASTEC Severe Accident Code : Description and Application to FPT-2 PHEBUS Test, *Nucl. Technol.*, 2010, **171**, 99–107.DOI: 10.13182/NT10-A10774.

13 L. Bosland, S. Dickinson, H. C. Glowa, G. A.Herranz, L. E.Kim, D. A. Powers, M. Salay and S. Tietze, Iodine-paint interactions during nuclear reactor severe accidents, *Ann. Nucl. Energy*, 2014, **74**, 184–199. DOI: 10.1016/j.anucene.2014.07.016.

14 M. Chebbi, B. Azambre, C. Volkringer and T. Loiseau, Dynamic sorption properties of Metal-Organic Frameworks for the capture of methyl iodide, *Microporous Mesoporous Mater.*, 2018, **259**, 244–254.DOI: 10.1016/j.micromeso.2017.10.018.

15 A. V Brenner, M. D. Tronko, M. Hatch, T. I. Bogdanova, V. A. Oliynik, J. H. Lubin, L. B. Zablotska, V. P. Tereschenko, R. J. Mcconnell, G. A. Zamotaeva, P. O. Kane, A. C. Bouville, L. V Chaykovskaya, E. Greenebaum, I. P. Paster, V. M. Shpak and E. Ron, I - 131 Dose Response for Incident Thyroid Cancers in Ukraine Related to the Chornobyl Accident, *Environ. Health Perspect.*, 2011, **119**, 933–939.DOI: 10.1289/ehp.1002674.

16 T. Ohba, T. Ishikawa, H. Nagai, S. Tokonami and A. Hasegawa, Reconstruction of residents ' thyroid equivalent doses from internal radionuclides after the Fukushima Daiichi nuclear power station accident, *Nat. Sci. reports*, 2020, **10**, 3639.DOI: 10.1038/s41598-020-60453-0.

17 G. Steinhauser, A. Brandl and T. E. Johnson, Comparison of the Chernobyl and Fukushima nuclear accidents: A review of the environmental impacts, *Sci. Total Environ.*, 2014, **470–471**, 800–817. DOI/ 10.1016/j.scitotenv.2013.10.029.

18 T. Imanaka, G. Hayashi and S. Endo, Comparison of the accident process , radioactivity release and ground contamination between Chernobyl and Fukushima-1, *J. Radiat. Res.*, 2015, **56**, 56–61. DOI: 10.1093/jrr/rrv074.

19 T.Christoudias and J. Lelieveld, Modelling the global atmospheric transport and deposition of radionuclides from the Fukushima Dai-ichi nuclear accident, *Atmos. Chem. Phys.*, 2013, **13**, 1425–1438. DOI: 10.5194/acp-13-1425-2013.

20 O. Masson, G. Steinhauser, H. Wershofen, H. W. Fischer, L. Pourcelot, O. Saunier, J. Bieringer, T. Steinkopff, M. Hýža, A. Dalheimer, A. de Vismes-Ott, K. Eleftheriadis, M. Forte, C. G. Leonarte, B. Møller, T. W. Bowyer and E. Dalaka, Potential Source Apportionment and Meteorological Conditions Involved in Airborne 131 I Detections in January/February 2017 in Europe, *Environ. Sci. Technol.*, 2018, **52**, 8488–8500. DOI: 10.1021/acs.est.8b01810.

21 M. Tombette, E. Quentric, D. Quélo, J. Benoit, A. Mathieu, I. Korsakissok and D. Didier, C3X : A software platform for assessing the consequences of an accidental release of radioactivity into the atmosphere, Poster, France, 2014. http://venus.iis.u-tokyo.ac.jp/English/workshop/Poster/3rd March/Damien Didier.pdf.

22 Y. Ando, K. Nishihara and H. Takano, Estimation of spent fuel compositions from light water reactors, *J. Nucl. Sci. Technol.*, 2000, **37**, 924–933. DOI: 10.1080/18811248.2000.9714974.

23 O. Saunier, I. Korsakissok, D. Didier, T. Doursout and A. Mathieu, Real-time use of inverse modeling techniques to assess the atmospheric accidental release from a nuclear power plant, *Radioprotection*, 2020, **55**, 107–115. DOI: 10.1051/radiopro/2020044.
24 C. Fortin, V. Fèvre-Nollet, F. Cousin, P. Lebègue and F. Louis, Box modelling of gas-phase atmospheric iodine chemical reactivity in case of a nuclear accident, *Atmos. Environ.,* 2019, **214**, 116838. DOI: 10.1016/j.atmosenv.2019.116838
25 V. Winiarek, M. Bocquet, O. Saunier and A. Mathieu, Estimation of errors in the inverse modeling of accidental release of atmospheric pollutant: Application to the reconstruction of the cesium-137 and iodine-131 source terms from the Fukushima Daiichi power plant, *J. Geophys. Res. Atmos.*, 2012, **117**, D05122. DOI: 10.1029/2011JD016932.
26 O. Masson, A. Baeza, J. Bieringer, K. Brudecki, S. Bucci, M. Cappai, F. P. Carvalho, O. Connan, C. Cosma, A. Dalheimer, D. Didier, G. Depuydt, L. E. De Geer, A. De Vismes, L. Gini, F. Groppi, K. Gudnason, R. Gurriaran, D. Hainz, Ó. Halldórsson, D. Hammond, O. Hanley, K. Holeý, Z. Homoki, A. Ioannidou, K. Isajenko, M. Jankovic, C. Katzlberger, M. Kettunen, R. Kierepko, R. Kontro, P. J. M. Kwakman, M. Lecomte, L. Leon Vintro, A. P. Leppänen, B. Lind, G. Lujaniene, P. Mc Ginnity, C. M. Mahon, H. Malá, S. Manenti, M. Manolopoulou, A. Mattila, A. Mauring, J. W. Mietelski, B. Møller, S. P. Nielsen, J. Nikolic, R. M. W. Overwater, S. E. Pálsson, C. Papastefanou, I. Penev, M. K. Pham, P. P. Povinec, H. Ramebäck, M. C. Reis, W. Ringer, A. Rodriguez, P. Rulík, P. R. J. Saey, V. Samsonov, C. Schlosser, G. Sgorbati, B. V. Silobritiene, C. Söderström, R. Sogni, L. Solier, M. Sonck, G. Steinhauser, T. Steinkopff, P. Steinmann, S. Stoulos, I. Sýkora, D. Todorovic, N. Tooloutalaie, L. Tositti, J. Tschiersch, A. Ugron, E. Vagena, A. Vargas, H. Wershofen and O. Zhukova, Tracking of airborne radionuclides from the damaged Fukushima Dai-Ichi nuclear reactors by European Networks, *Environ. Sci. Technol.*, 2011, **45**, 7670–7677. DOI: 10.1021/es2017158.
27- A. Laskin, R. C. Moffet, M. K. Gilles, J. D. Fast, R. A. Zaveri, B. Wang, P. Nigge, J. Shutthanandan, Tropospheric chemistry of internally mixed sea salt and organic particles: Surprising reactivity of NaCl with weak organic acids, *J. Geophys. Res. Atmos*, 2012, **117**, D15302. DOI:10.1029/2012JD017743
28 J. W.Chi, W. J. Li, D. Z. Zhang, J. C. Zhang, Y. T. Lin, X. J. Shen, J. Y. Sun, J. M. Chen, X. Y. Zhang, Y. M. Zhang, W. X. Wang, W. X., Sea salt aerosols as a reactive surface for inorganic and organic acidic gases in the Arctic troposphere, *Atmos. Chem. Phys.*, 2015, **15**, 11341–11353. DOI: 10.5194/acp-15-11341-2015
29 R. Vogt and B. J. Finlayson-Pitts, A Diffuse Reflectance Infrared Fourier Transform Spectroscopic (DRIFTS) study of the surface reaction of NaCl with gaseous NO2 and HN03, *J. Phys. Chem.*, 1994, **98**, 3747–3755. DOI: 10.1021/j100065a033
30 J. Sirita, S. Phanichphant and F. C. Meunier, Quantitative analysis of adsorbate concentrations by diffuse reflectance FT-IR, *Anal. Chem.*, 2007, **79**, 3912–3918.DOI: 10.1021/ac0702802.
31 C. Lentz, S. P. Jand, J. Melke, C. Roth and P. Kaghazchi, Journal of Molecular Catalysis A : Chemical DRIFTS study of CO adsorption on Pt nanoparticles supported by DFT calculations, *J. Mol. Catal. A. Chem.*, 2017, **426**, 1–9. DOI: 10.1021/ac0702802
32 M. Gouello, Thèse de doctorat, Chimie de l'iode et composition des aérosols dans le circuit primaire d'un réacteur nucléaire en situation d'accident grave, Université de Grenoble, 2013.
33 C. Su, J. C. Yeh, C. C. Chen, J. C. Lin and J. L. Lin, Study of adsorption and reactions of methyl iodide on TiO_2, *J. Catal.*, 2000, **194**, 45–54.DOI: 10.1006/jcat.2000.2909
34 M. Chebbi, B. Azambre, L. Cantrel and A. Koch, A Combined DRIFTS and DR-UV-Vis Spectroscopic *in Situ* Study on the Trapping of CH_3I by Silver-Exchanged Faujasite Zeolite, J. *Phys. Chem. C*, 2016, **120**, 18694–18706.
DOI: 10.1021/acs.jpcc.6b07112.
35 M. L. Colaianni, P. J. Chen, H. Gutleben and J. T. Yates, Vibrational studies of CH_3I on Si(100)-(2×1): adsorption and decomposition of the methyl species, *Chem. Phys. Lett.*, 1992, **191**, 561–568. DOI: 10.1016/0009-2614(92)85589-3.
36 C. J. Jenks, B. E. Bent, N. Bernstein and F. Zaera, The Chemistry of Alkyl Iodides on Copper Surfaces, *Phys. Chem. B*, 2000, **104**, 3008–3016. DOI: 10.1021/jp993021s.
37 M. A. Henderson, G. E. Mitchell and J. M. White, The chemisorption of methyl halides (Cl, Br and I) on Pt(111), *Surf. Sci. Lett.*, 1987, **184**, 325–331.
DOI: 10.1016/0167-2584(87)90754-7
38 F. Solymosi and G. Klivényi, HREELS study of CH_3I and CH_3 adsorbed on Rh(111) surface, *J. Electron Spectros. Relat. Phenomena,* 1993, **64/65**, 499–506.DOI: 10.1016/0368-2048(93)80115-3
39 J. Lin and B. E. Bent, Iodomethane dissociation on Cu(111): Bonding and chemistry of adsorbed methyl groups, *J. Vac. Sci. Technol. A,* 1992, **10**, 2202–2209. DOI: 10.1116/1.578005.
40 G. Klivényi and F. Solymosi, Generation of CH_2 species: thermal and photo-induced dissociation of CH_2I_2 on Rh(111) surface, *Surf. Sci.*, 1995, **342**, 168–184. DOI: 10.1016/0039-6028(95)00767-9.
41 M. K. Weldon and C. M. Friend, Spectroscopic characterization of surface methylene on Mo(110), *Surf. Sci.,*1994, **321**, L202-L208. DOI:10.1016/0039-6028(94)90175-9.
42 K. C. Scheer, A. Kis, J. Kiss and J. M. White, Adsorption and reactions of CH_2I_2 on clean and oxygen-modified Ag (111): a RAIRS and TPD study, *Top. Catal.*, 2002, **20**, 43–51.DOI: 10.1023/A:1016395214602
43 T. Makino, S. Zulaehah, J. S. Gueriba, W. A. Diño and M. Okada, CH_3Cl/Cu(410): Interaction and Adsorption Geometry, *J. Phys. Chem. C*, 2018, **122**, 1.1825–11831. DOI: 10.1021/acs.jpcc.8b01296.

44 J.Cserenyi, L. Ovari, T. Bansagi and F. Solymosi, Adsorption and reactions of CH_3Cl on Mo_2C based catalyst, *J. Mol. Catal. A: Chem.*, 2000, **162,** 335–352. DOI: 10.1016/S1381-1169(00)00301-0.
45 M. Gu, X. Liu, L. Yang, S. Sun and J. Zhang, Dynamics of $Cl^-(H_2O)$ + CH_3I Substitution Reaction: The Influences of Solvent and Nucleophile, J. *Phys. Chem. A.,* 2019, **123**, 2203-2210. DOI: 10.1021/acs.jpca.9b00348.
46 A.Saiz-Lopez, J. M. C. Plane, A. S. Mahajan, P. S. Anderson, A. E. Jones, H. K. Roscoe, R. A. Salmon, W. J. Bloss and J. D. Lee, On the vertical distribution of boundary layer halogens over coastal Antarctica : implications for O_3 , HO_x , NO_x and the Hg lifetime, *Atmos. Chem. Phys.*, **2008**, 8, 887–900. DOI: 10.5194/acp-8-887-2008.
47 L. D. Kong, X. Zhao, Z. Y. Sun, Y. W. Yang, H. B. Fu, S. C. Zhang, T. T. Cheng, X. Yang, L. Wang and J. M. Chen, The effects of nitrate on the heterogeneous uptake of sulfur dioxide on hematite, *Atmos. Chem. Phys.*, 2014, **14**, 9451–9467.DOI: 10.5194/acp-14-9451-2014.
48 H. J. Li, T. Zhu, D. F. Zhao, Z. F. Zhang and Z. M. Chen, Kinetics and mechanisms of heterogeneous reaction of NO_2 on $CaCO_3$ surfaces under dry and wet conditions, *Atmos. Chem. Phys.*, 2010, **10**, 463–474. DOI: 10.5194/acp-10-463-2010.
49 M. Ullerstam, M. S. Johnson, R. Vogt and E. Ljungström, DRIFTS and Knudsen cell study of the heterogeneous reactivity of SO_2 and NO_2 on mineral dust, *Atmos. Chem. Phys. Discuss.,* 2003, **3**, 4069–4096. DOI: 10.5194/acp-3-2043-2003.
50 A. Allanic and M. J. Rossi, Heterogeneous reactions of HOI on substrates of atmospheric importance, *Geophys. Res. Lett.*, 1999, **104**, 18689–18696.DOI: 10.1029/1999JD900285.